Formation of electron energy spectra during magnetic reconnection in laser-produced plasma

Kai Huang, Quanming Lu, Can Huang, Quanli Dong, Huanyu Wang, Feibin Fan, Zhengming Sheng, Shui Wang, and Jie Zhang

Citation: Physics of Plasmas **24**, 102101 (2017); doi: 10.1063/1.4994260
View online: http://dx.doi.org/10.1063/1.4994260
View Table of Contents: http://aip.scitation.org/toc/php/24/10
Published by the American Institute of Physics

Formation of electron energy spectra during magnetic reconnection in laser-produced plasma

Kai Huang,[1,2] Quanming Lu,[1,2,a)] Can Huang,[1,2] Quanli Dong,[3,4] Huanyu Wang,[1,2] Feibin Fan,[1,2] Zhengming Sheng,[4,5,6] Shui Wang,[1,2] and Jie Zhang[4,5]
[1]*CAS Key Laboratory of Geospace Environment, Department of Geophysics and Planetary Science, University of Science and Technology of China, Hefei 230026, China*
[2]*Collaborative Innovation Centers of Astronautical Science and Technology, Harbin, China*
[3]*School of Physics and Optoelectronic Engineering, Ludong University, Yantai 264025, China*
[4]*Innovative Collaboration Center of IFSA, Shanghai Jiao Tong University, Shanghai 200240, China*
[5]*MoE Key Laboratory for Laser Plasmas and School of Physics and Astronomy, Shanghai Jiao Tong University, Shanghai 200240, China*
[6]*SUPA, Department of Physics, University of Strathclyde, Glasgow G4 0NG, United Kingdom*

(Received 5 July 2017; accepted 21 August 2017; published online 12 September 2017)

Energetic electron spectra formed during magnetic reconnection between two laser-produced plasma bubbles are investigated by the use of two-dimensional particle-in-cell simulations. It is found that the evolution of such an interaction between the two plasma bubbles can be separated into two distinct stages: squeezing and reconnection stages. In the squeezing stage, when the two plasma bubbles expand quickly and collide with each other, the magnetic field in the inflow region is greatly enhanced. In the second stage, a thin current sheet is formed between the two plasma bubbles, and then, magnetic reconnection occurs therein. During the squeezing stage, electrons are heated in the perpendicular direction by betatron acceleration due to the enhancement of the magnetic field around the plasma bubbles. Meanwhile, non-thermal electrons are generated by the Fermi mechanism when these electrons bounce between the two plasma bubbles approaching quickly and get accelerated mainly by the convective electric field associated with the plasma bubbles. During the reconnection stage, electrons get further accelerated mainly by the reconnection electric field in the vicinity of the X line. When the expanding speed of the plasma bubbles is sufficiently large, the formed electron energy spectra have a kappa distribution, where the lower energy part satisfies a Maxwellian function and the higher energy part is a power-law distribution. Moreover, the increase in the expanding speed will result in the hardening of formed power-law spectra in both the squeezing and reconnection stages. *Published by AIP Publishing.*
[http://dx.doi.org/10.1063/1.4994260]

I. INTRODUCTION

Magnetic reconnection is a fundamental process allowing topological changes in magnetic field lines and rapid conversion of magnetic energy into plasma kinetic and thermal energies. It is suggested that many kinds of explosive phenomena in plasmas, such as solar flares,[1,2] magnetosphere substorms,[3–5] and sawtooth crash in tokamaks,[6,7] are related to magnetic reconnection. The production of energetic electrons is also a significant feature of magnetic reconnection. For example, in solar flares, up to 50% of energy release can appear as energetic electrons,[8,9] which in general have a power-law spectrum. Electron acceleration during magnetic reconnection has been extensively studied in recent years. Electrons can be accelerated by the reconnection electric field around the X line[10–15] and in the jet front by the betatron and Fermi mechanisms.[16–19] Magnetic islands have also been considered to play an important role in electron acceleration during magnetic reconnection. Electrons can get accelerated when they are trapped and reflected at the two ends of an island[11,20,21] and in the merging region when two islands begin to coalesce,[22–25] while both simulations and observations have shown that the coalescence of magnetic islands should be a common phenomenon during magnetic reconnection.[26–29] Although much effort has been made to understand the process of electron acceleration during magnetic reconnection, how a power-law spectrum of energetic electrons is generated is still a mystery.[30]

Recently, several experiments of magnetic reconnection in a high-energy-density (HED) laser-produced plasma have been conducted at laser facilities Vulcan,[31–33] OMEGA,[34,35] and Shenguang-II.[36,37] In these experiments, two pulses of high power laser beams are focused on a planar foil target, the target is suddenly ionized, and two plasma bubbles are formed. The two plasma bubbles expand at a supersonic speed, and the toroidal magnetic field is generated around the plasma bubbles. The two plasma bubbles collide with each other, and magnetic reconnection occurs in the squeezing region. Different from magnetic reconnection in a Harris current sheet, before the development of the reconnection of toroidal magnetic field lines associated with the two laser-produced plasma bubbles, the magnetic field in the inflow region is greatly enhanced due to the squeezing of the two plasma bubbles,[38–40] which expand with a speed much higher that the Alfvén speed.

a)Author to whom correspondence should be addressed: qmlu@ustc.edu.cn

Both experiments and particle-in-cell (PIC) simulations have demonstrated the production of energetic electrons during magnetic reconnection in a laser-produced plasma, and usually, these electrons have power-law spectra.[37,41] By performing two-dimensional (2-D) PIC simulations, Lu *et al.*[42] investigated the process of electron acceleration during magnetic reconnection in a laser-produced plasma and found that besides the reconnection electric field, Fermi and betatron mechanisms also play an important role during the expanding stage. The electrons in the magnetic ribbons are energized through the betatron mechanism due to the enhancement of the magnetic field, while the Fermi mechanism takes the effect when electrons are trapped and bounced repeatedly between the two expanding bubbles. However, it is still in debate regarding how a power-law spectrum of energetic electrons is formed in the presence of a laser-produced plasma. In this paper, with the use of 2-D PIC simulations, we investigate what the roles of the reconnection electric field, betatron, and Fermi mechanisms play in the formation of the electron energy spectra during magnetic reconnection in a laser-produced plasma.

This paper is organized as follows: In Sec. II, we describe the simulation model. In Sec. III, the simulation results are presented. Finally, conclusions and discussion are given in Sec. IV.

II. SIMULATION MODEL

In our 2-D PIC simulation model, the electromagnetic field is defined on the grids and updated by solving Maxwell's equations with a full explicit algorithm. Ions and electrons are relativistically advanced in the electromagnetic field. The laser-plasma interaction and generation process of the magnetic field are not involved in our simulations, and the initial conditions in the simulations are set corresponding to the plasma bubble expanding phase in the experiment. The conditions are similar to those in previous works:[38–40] two circular plasma bubbles are defined in the (x, y) plane with the toroidal magnetic field around them. The simulation domain size is $[-L_x, L_x] \times [-L_y, L_y]$, and the centers of the two plasma bubbles are $(0, -L_0)$ and $(0, L_0)$. The radius vectors from the center of each plasma bubble are defined as $\mathbf{r}^{(1)} = (x, y + L_0)$ and $\mathbf{r}^{(2)} = (x, y - L_0)$.

There are two kinds of magnetic field geometry in our simulations: AP case (with reconnection) and P case (without reconnection). The magnetic field is initialized as the sum of two toroidal ribbons: $\mathbf{B}^{(1)} + \mathbf{B}^{(2)}$. In the AP case, the magnetic field is defined as

$$\mathbf{B}^{(i)}(\mathbf{r}) = \begin{cases} \mathbf{B}_0 \sin\left(\dfrac{\pi(L_n - r^{(i)})}{2L_B}\right)\hat{\mathbf{r}}^{(i)} \times \hat{\mathbf{z}} & r^{(i)} \in [L_n - 2L_B, L_n] \\ 0 & \textit{otherwise}. \end{cases} \tag{1}$$

Here, L_n is the radius of the two bubbles, where $L_n < \min\{L_0, L_x\}$ and $L_0 + L_n < L_y$, so the simulation domain can contain two whole bubbles. L_B is the half width of the initial magnetic ribbons. In the P case, the magnetic field is

$$\mathbf{B}^{(i)}(\mathbf{r}) = \begin{cases} \mathbf{B}_0 \sin\left(\dfrac{\pi(L_n - r^{(1)})}{2L_B}\right)\hat{\mathbf{r}}^{(1)} \times \hat{\mathbf{z}} & r^{(1)} \in [L_n - 2L_B, L_n] \\ 0 & \textit{otherwise} \\ -\mathbf{B}_0 \sin\left(\dfrac{\pi(L_n - r^{(2)})}{2L_B}\right)\hat{\mathbf{r}}^{(2)} \times \hat{\mathbf{z}} & r^{(2)} \in [L_n - 2L_B, L_n]. \end{cases} \tag{2}$$

An initial out-of-plane current is added to satisfy Ampere's law. The initial density is $n_b + n^{(1)} + n^{(2)}$, where n_b is the background density and $n^{(i)}(i = 1, 2)$ is the density of each bubble, which is defined as

$$n^{(i)}(\mathbf{r}) = \begin{cases} (n_0 - n_b)\cos^2\left(\dfrac{\pi r^{(i)}}{2L_n}\right) & r^{(i)} < L_n \\ 0 & \textit{otherwise}, \end{cases} \tag{3}$$

where n_0 is the peak density of the bubbles, and we choose $n_b = 0.1n_0$. The initial expanding velocity of the plasma bubbles is $\mathbf{V}^{(1)} + \mathbf{V}^{(2)}$, and $\mathbf{V}^{(i)}(i = 1, 2)$ is

$$\mathbf{V}^{(i)}(\mathbf{r}) = \begin{cases} V_0 \sin\left(\dfrac{\pi r^{(i)}}{L_n}\right)\hat{\mathbf{r}}^{(i)} & r^{(i)} < L_n \\ 0 & \textit{otherwise}, \end{cases} \tag{4}$$

where V_0 is the initial expanding speed of the two plasma bubbles.

To be consistent with the plasma flow, an initial electric field $\mathbf{E} = -\mathbf{V} \times \mathbf{B}$ is imposed. The expanding speed of the plasma bubbles is usually supersonic, and in experiments, the sonic Mach number is $M_s = V_0/c_s = 2 - 8$[43,44] (where $c_s\left(= \sqrt{\gamma Z T_e/m_i}\right)$ is the sound speed, and Z is the ion charge). To study the influence of the expanding speed on the electron energy spectrum, we run 5 sub-cases for both the AP case and P case. The expanding speeds of the five cases are set to be $V_0/c_s = 2$, 3, 4, 5, and 6. The sound speed c_s is equal to $1.545v_A$ (where v_A is the Alfvén speed based on n_0 and B_0) in our simulations.

The size of the plasma bubbles is $L_n = 12d_i$ in our simulations and $L_B = 2d_i$, where $d_i = c/\omega_{pi}$ is the ion inertial length based on n_0. L_0 is set to be $12.5d_i$. The ion-to-electron mass ratio Zm_i/m_e is 100, and the light speed is $c = 75v_A$. The initial temperatures of ions and electrons are set to be uniform $T_i = T_e = 0.025m_e c^2$, and their initial velocity distributions are Maxwellian with the bulk velocities in the radial direction and drift velocities in the z direction to supply the out-of-plane current. The plasma beta is $\beta_e = \beta_i = 2\mu_0 n_0 k_B T_e/B_0^2 \approx 2.9$. In the simulations, $L_x = 25d_i$ and $L_y = 35d_i$, and the number of grid points is $N_x \times N_y = 1000 \times 1400$ with a spatial resolution of $\Delta x = \Delta y = 0.05d_i$. The time step is $\Delta t = 0.0001\Omega_i^{-1}$, where $\Omega_i = eB_0/m_i$ is the ion gyrofrequency. 2560 particles per species in a grid for n_0 are employed in the simulations. The periodic boundary conditions for both the x and y directions are used.

III. SIMULATION RESULTS

Let us at first analyze the evolution of the interaction between two plasma bubbles expanding with a supersonic speed. Figure 1 shows the magnetic field B/B_0 and the out-of-plane electron current density J_{ez}/en_0v_A at $\Omega_i t = 0$, 0.3, 0.55, and 0.75 for (a) AP and (b) P cases, and here, the expanding speed is $V_0/c_s = 5$. Initially, the evolution of the AP case is similar to that of the P case. The two plasma bubbles expand with a supersonic speed and approach together quickly. At the same time, the magnetic field surrounding the plasma bubbles is greatly enhanced due to the expanding of the plasma bubbles, especially in the inflow region where the plasma bubbles suffer a strong squeezing. However, in the AP case, a thin electron current sheet is formed between the two plasma bubbles at about $\Omega_i t = 0.55$, and then, at about $\Omega_i t = 0.58$, the reconnection of magnetic field lines associated with the two plasma bubbles occurs. Therefore, the interaction between the two plasma bubbles in the AP system can be roughly divided into two stages, i.e., the squeezing stage and the reconnection stage. While in the P case, we can only observe the squeezing between the two plasma bubbles. The two stages of the interaction between the two plasma bubbles in the AP case with $V_0/c_s = 5$ can be distinguished more clearly in Fig. 2, where the time evolution of reconnected magnetic flux Φ_B/B_0d_i, the maximum of the upstream magnetic field $B_{\max}/B_0$, and the reconnection electric field E_z/v_AB_0 at $(x, y) = (0, 0)$ are plotted. The evolution of the maximum of the upstream magnetic field $B_{\max}/B_0$ in the P case with $V_0/c_s = 5$ is also shown for reference. Before about $\Omega_i t = 0.45$, the maximum of the upstream magnetic field in the AP case is almost the same as that in the P case. It means that during this time period, there is only squeezing between the two plasma bubbles, and no reconnection occurs. The maximum of the upstream magnetic field reached its peak at about $\Omega_i t = 0.6$ in the AP case, while in the P case, the peak is attained at about $\Omega_i t = 0.75$. In the AP case, at about $\Omega_i t = 0.6$, the pileup rate of the magnetic flux is equal to the reconnection rate, and about only 25% of the total

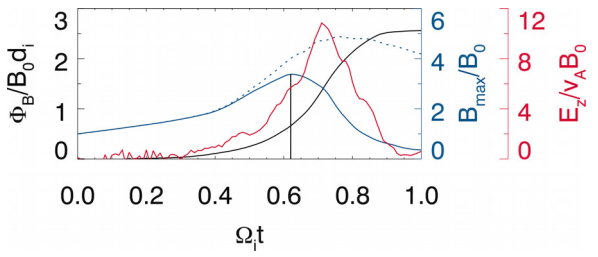

FIG. 2. Time evolution of the reconnected magnetic flux Φ_B/B_0d_i, the out-of-plane electric field E_z/v_AB_0 at $(x, y) = (0, 0)$, and the maximum of the upstream magnetic field $B_{\max}/B_0$ in the AP case (blue full line). The maximum of the upstream magnetic field $B_{\max}/B_0$ in the P case (blue dashed line) is also plotted. Here, the expanding speed is $V_0/c_s = 5$.

magnetic flux has been reconnected. Therefore, in the AP case, we can use the time when the maximum of the upstream magnetic field reaches its peak to separate the squeezing stage and the reconnection stage. Before that time, the interaction of two plasma bubbles is dominated by the squeezing, while magnetic reconnection becomes important only after $\Omega_i t = 0.6$. Similar results are obtained in Ref. 45.

Figure 3 describes the electron energy spectra at different times for different expanding speeds $V_0/c_s = 2$, 3, 4, 5, and 6. Here, $\Omega_i t =$ 1.2, 0.95, 0.75, 0.6, and 0.53 correspond to the times when the maximum of the upstream magnetic field reaches its peak in the AP cases for $V_0/c_s = 2$, 3, 4, 5, and 6, respectively, while $\Omega_i t =$ 1.7, 1.2, 0.9, 0.79, and 0.65 correspond to the times when the flux of non-thermal electrons reaches its peak in AP cases for $V_0/c_s = 2$, 3, 4, 5, and 6, respectively. In order to compare the results in AP cases with those in P cases, the electron energy spectra at the same times in P cases as those in AP cases are also plotted in the figure. Here, when we calculate the electron spectra, only the electrons in the ribbons of magnetic field ($r^{(i)} \in [L_n - 2L_B, L_n]$) are included. The reason for this is that during the magnetic reconnection experiment in a laser-driven plasma, the background plasma is usually negligible and the plasma in the center of plasma bubbles is not involved in magnetic reconnection. Also,

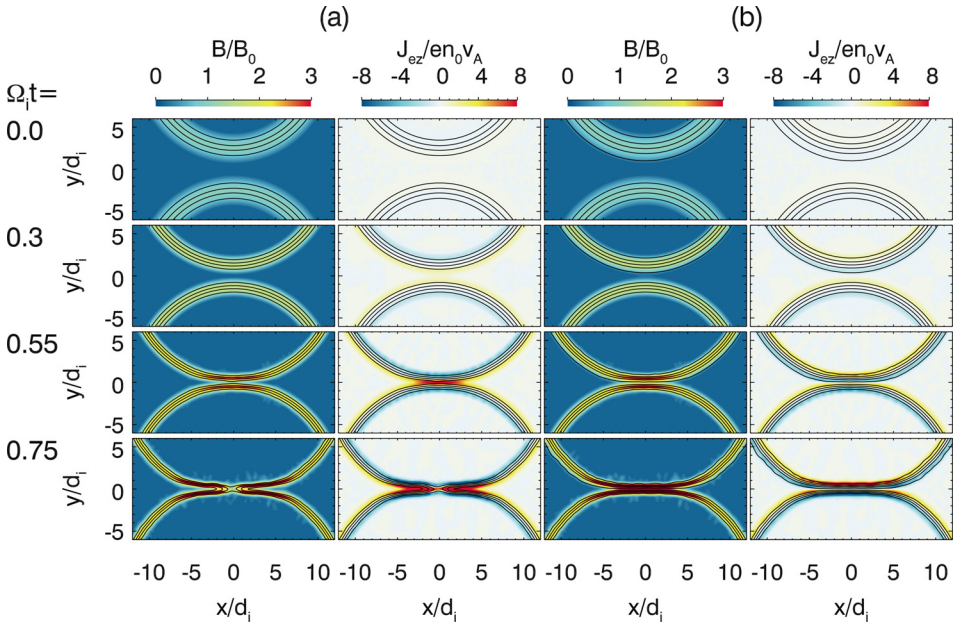

FIG. 1. The magnetic field B/B_0 and out-of-plane electron current density J_{ez}/en_0v_A at $\Omega_i t = 0$, 0.3, 0.55, and 0.75 in the AP case (a) and P case (b). The expanding speed is $V_0/c_s = 5$.

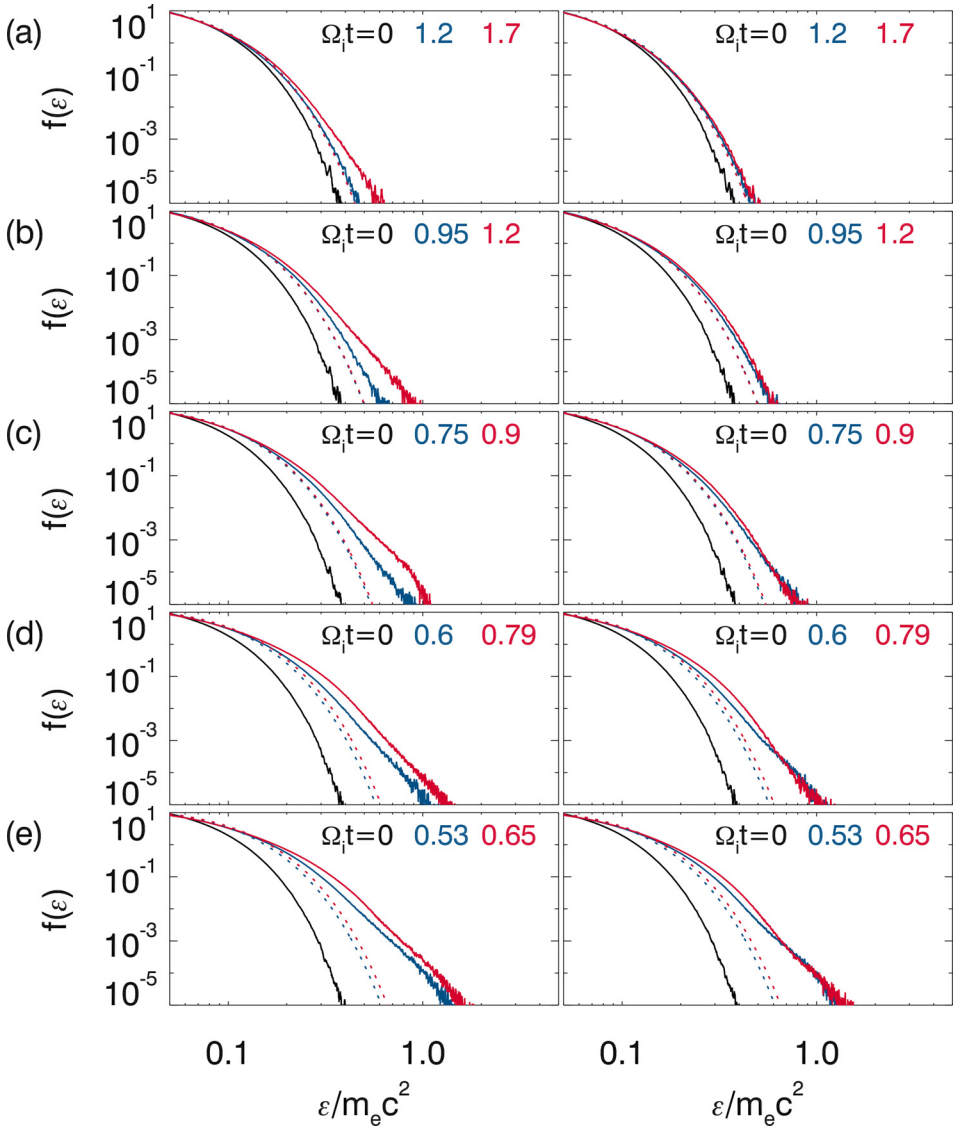

FIG. 3. Electron energy spectra in AP and P cases for different expanding speeds V_0/c_s =(a) 2, (b) 3, (c) 4, (d) 5, and (e) 6. The spectra in the left column correspond to those in AP cases, while those in the right column correspond to those in P cases. The black lines represent the initial spectra, the blue lines represent the spectra when the maximum of the upstream magnetic field reaches its peak in AP cases, and the red lines represent the spectra when the flux of non-thermal electrons reaches its peak in AP cases. The blue dotted and red lines correspond to the Maxwellian distributions fitted from the blue and red lines, respectively.

when an electron leaves the boundary of the simulation domain, its energy will be kept unchanged during the calculation of electron energy spectra. In both AP and P cases, we can find that the formed electron energy spectra satisfy the kappa distribution when the expanding speed is sufficiently large. In the lower energy part, the electron energy spectra satisfy the Maxwellian distribution, where the temperature increases with the increase in the expanding speed; in the higher energy part, the electron energy spectra satisfy the power-law distribution, which becomes harder and harder with the increase in the expanding speed. The electron energy spectra in the squeezing stage of AP cases are similar to those at the corresponding times of P cases. In AP cases, the indices of power-law distribution in the higher energy are 7.3, 6.9, and 5.5 for $V_0/c_s = 4$, 5, and 6, respectively, while they are 8.2, 6.2, and 5.9 in P cases. It means that at the squeezing stage of AP cases, the mechanism of electron acceleration is similar to that in P cases. Electrons can be further accelerated at the reconnection stage of AP cases with the increase in energetic electron flux, and the electron energy spectra are harder than those at the corresponding times of P cases. In AP cases, the indices of power-law distribution in higher energy are 5.7, 6.4, and 5.7 for $V_0/c_s = 4$, 5, and 6, respectively, while they are 9.4, 7.5, and 6.3 in P cases. Therefore, at the reconnection stage of AP cases, the reconnection electric field plays an important role in electron acceleration, but with the increase in the expanding speed, the reconnection electric field become less and less important.

Detailed analysis shows that at the squeezing stage of AP cases, the electron parallel temperature changes little, while the corresponding perpendicular temperature increases. Figure 4 shows the electron perpendicular temperature in AP cases versus the average magnetic field in the magnetic ribbons around the plasma bubbles for different expanding speeds $V_0/c_s = 2$, 3, 4, 5, and 6. The perpendicular temperature increases with the increase in the expanding speed, and it almost satisfies that $T_\perp/B$ is a constant. Therefore, we can conclude that at the squeezing stage of AP cases, the increase in electron temperature is caused by the betatron mechanism, where the magnetic momentum is a constant. At the same time, we also find that the increase in electron temperature in P cases is also caused by the betatron mechanism.

Figure 5 shows a typical electron trajectory at the squeezing stage of the AP case with $V_0/c_s = 5$: (a) the electron position in the simulation domain, (b) the electron energy versus

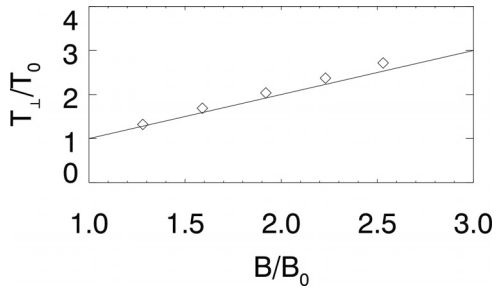

FIG. 4. The relationship between the perpendicular temperature of electrons and the average enhancement of the magnetic field at the magnetic ribbons around the plasma bubbles in the AP case at times when the maximum of the upstream magnetic field reaches its peak. From left to right, the five diamond symbols refer to the cases where $V_0/c_s = 2$, 3, 4, 5, and 6 respectively. The full line represents $T_\perp/T_0 = B_{ave}/B_0$.

the electron position in the y direction, (c) the time evolution of electron energy, the works done by the convective electric field $-\mathbf{u}_i \times \mathbf{B}$ and non-ideal electric field $\mathbf{E} + \mathbf{u}_i \times \mathbf{B}$, and (d) the electron position in the (y, z) plane, where the z position is calculated by $\int v_z dt$. Obviously, the electron bounces between the two plasma bubbles approaching quickly, and during this time period, the electron moves about 10 ion inertial lengths along the z direction. Every time, the electron gets accelerated when it is reflected by the plasma bubbles, and it is accelerated mainly by the convective electric field. Therefore, we can conclude that the energetic electrons at the squeezing stage of AP cases are accelerated by the Fermi mechanism. For comparison, Fig. 6 shows a typical electron trajectory in the P case with $V_0/c_s = 5$. Similar to that at the squeezing stage of the AP case, the electron suffers Fermi acceleration when it

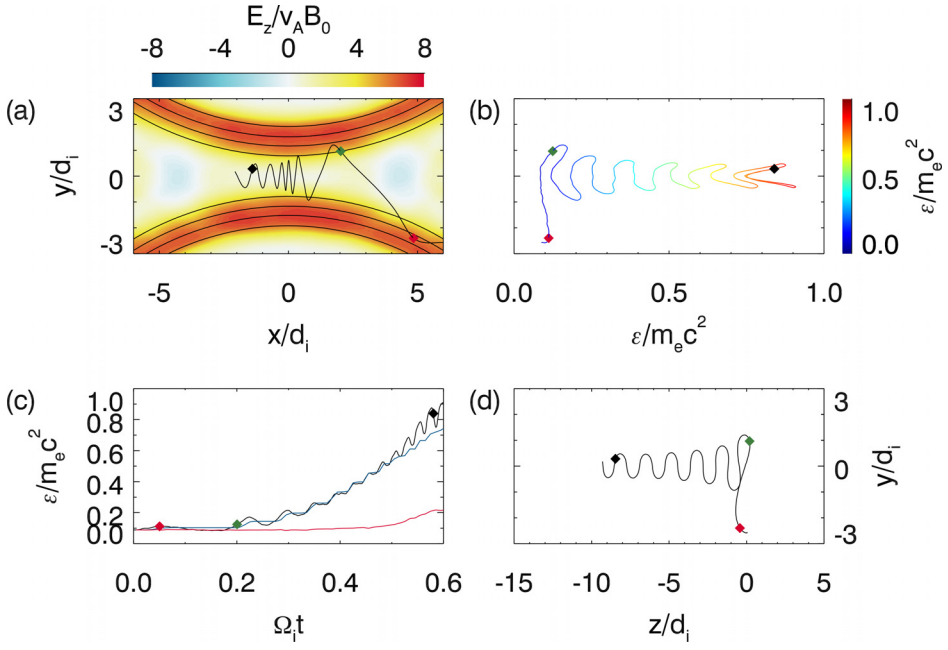

FIG. 5. (a) The trajectory of a non-thermal electron produced by the Fermi mechanism during $\Omega_i t = 0$ and 0.6 in the AP case, the expanding speed is $V_0/c_s = 5$, and the magnetic field lines and the out-of-plane electric field at $\Omega_i t = 0.3$ are plotted for reference. (b) The electron's energy versus its position in the y direction. The color of the trajectory also represents the electron energy. (c) The black line shows the evolution of the electron energy, and the blue and red lines show the works done by the convective electric field $-\mathbf{u}_i \times \mathbf{B}$ (where $\mathbf{u}_i$ is the ion bulk velocity) and non-ideal electric field $\mathbf{E} + \mathbf{u}_i \times \mathbf{B}$, respectively. (d) The electron trajectory in the (z, y) plane, where the z position is calculated by $\int_0^\tau v_z dt$. The red, green, and black full diamonds represent $\Omega_i t = 0.05$, 0.2, and 0.58 respectively.

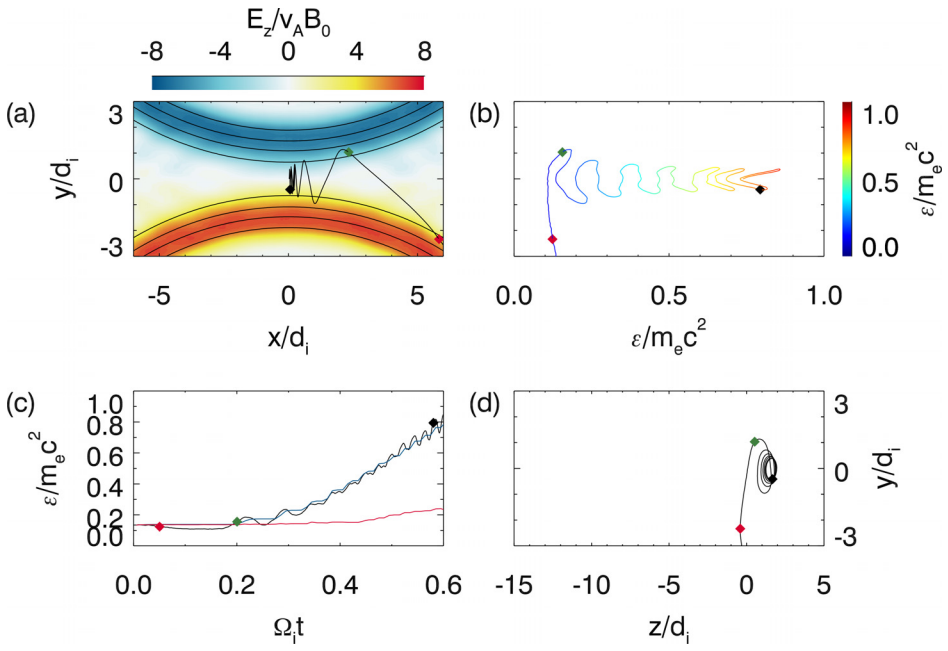

FIG. 6. (a) The trajectory of a non-thermal electron produced by Fermi acceleration at $\Omega_i t = 0$ and 0.6 in the P case, the expanding speed is $V_0/c_s = 5$, and the magnetic field lines and the out-of-plane electric at $\Omega_i t = 0.3$ are plotted for reference. (b) The electron's energy versus its position in the y direction. The color of the trajectory also represents the electron energy. (c) The black line shows the evolution of the electron energy, and the blue and red lines show the works done by the convective electric field $-\mathbf{u}_i \times \mathbf{B}$ and non-ideal electric field $\mathbf{E} + \mathbf{u}_i \times \mathbf{B}$, respectively. (d) The electron trajectory in the (z, y) plane, where the z position is calculated by $\int_0^\tau v_z dt$. The red, green, and black full diamonds represent $\Omega_i t = 0.05$, 0.2, and 0.58 respectively.

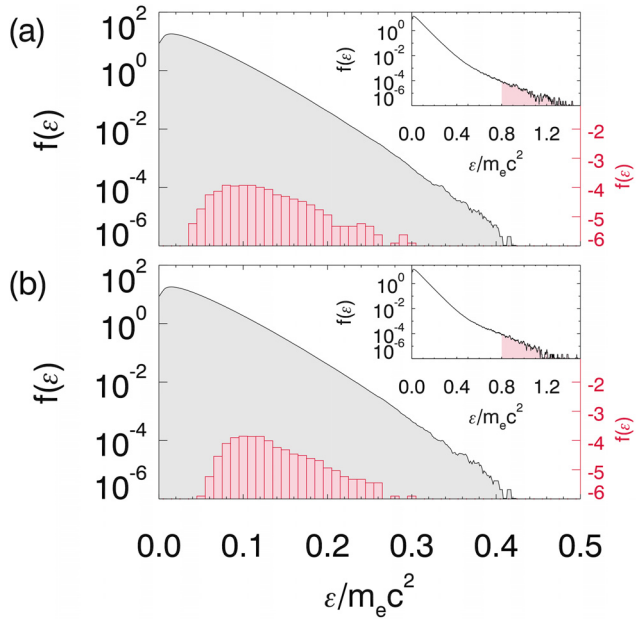

FIG. 7. The initial energy distributions of electrons whose energy exceeds $0.8m_ec^2$ at $\Omega_i t = 0.6$ (at the end of the squeezing stage) in the AP case (a) and P case (b) and is denoted by red color. The initial electron energy spectra are plotted for reference (black color), and the energy distributions of these electrons at $\Omega_i t = 0.6$ are plotted at the top right corner of each subgraph. The expanding speed is $V_0/c_s = 5$.

bounces between the two plasma bubbles. The difference is that in the P case, the electron only moves about 2 ion inertial lengths along the z direction.

Figure 7 shows initial electron energy distributions, where the energy of these electrons exceeds $0.8m_ec^2$ at $\Omega_i t = 0.6$ for AP and P cases with $V_0/c_s = 5$. We can find that the initial electron energy distributions in both cases are similar, and only the electrons with the initial energy higher than about $0.03m_ec^2$ (corresponding to an electron with a velocity of 10 $v_A \approx 6.5\ c_s$, larger than the expanding speed $V_0/c_s = 5$) can be accelerated to very high energy by the Fermi mechanism.

Figure 8 plots a typical electron trajectory, which is accelerated at the reconnection stage of the AP case with $V_0/c_s = 5$: (a) the electron position in the simulation domain, (b) the electron energy versus the electron position in the y direction, (c) the time evolution of electron energy, the works done by the convective electric field $-\mathbf{u}_i \times \mathbf{B}$ and non-ideal electric field $\mathbf{E} + \mathbf{u}_i \times \mathbf{B}$, and (d) the electron position in the (y, z) plane, where the z position is calculated by $\int v_z dt$. At about $\Omega_i t = 0.6$, the electron enters the diffusion region and is accelerated by the non-ideal electric field. Different from that in the Fermi acceleration, the work done by the convective electric field is negligible to accelerate the electron. It is noted that the electron moves about 10 ion inertial lengths along the z direction, close to that in the Fermi process. Both the Fermi mechanism and reconnection electric field should play important roles to accelerate electrons in a three-dimensional situation.

Figure 9 shows the electron energy distributions at $\Omega_i t = 0.6$, where the energy of these electrons exceeds $1.0m_ec^2$ at $\Omega_i t = 0.79$ for AP and P cases with $V_0/c_s = 5$. There are essential differences between AP and P cases. In P cases, the electrons only suffer the Fermi acceleration. In the AP case, the energy of most of these electrons at $\Omega_i t = 0.6$ is lower than $0.8m_ec^2$, and there is no energy threshold for electrons to be accelerated to higher than $1.0m_ec^2$ at $\Omega_i t = 0.79$. Only a small part of these electrons have energy higher than $0.8m_ec^2$ at $\Omega_i t = 0.6$. It means that most of these energetic electrons only suffer acceleration by the reconnection electric field, and only a small part is accelerated by both Fermi and reconnection electric fields.

IV. CONCLUSIONS AND DISCUSSION

In this paper, we investigated the evolution of electron energy spectra during magnetic reconnection in a laser-produced plasma by the use of 2-D PIC simulations. The interaction between the two plasma bubbles expanding with supersonic speed can be divided into squeezing and reconnection stages.

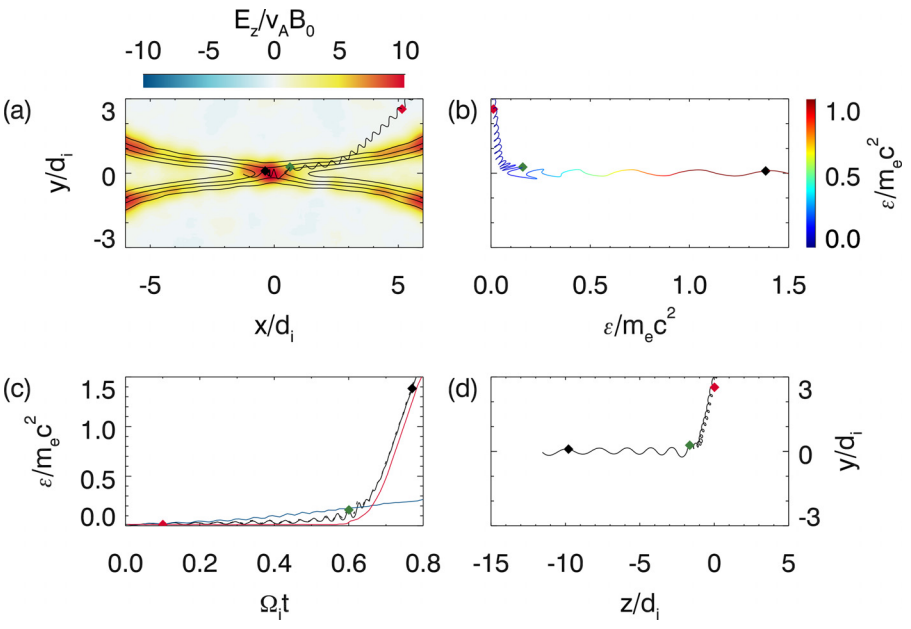

FIG. 8. (a) The trajectory of a non-thermal electron produced at the reconnection stage during $\Omega_i t = 0$ and 0.8 in the AP case, the expanding speed is $V_0/c_s = 5$, and the magnetic field lines and the out-of-plane electric field at $\Omega_i t = 0.7$ are plotted for reference. (b) The electron's energy versus its position in the y direction. The color of the trajectory also represents the electron energy. (c) The black line shows the energy evolution of this electron, and the blue and red lines show the works done by the convective electric field $-\mathbf{u}_i \times \mathbf{B}$ and non-ideal electric field $\mathbf{E} + \mathbf{u}_i \times \mathbf{B}$, respectively. (d) The electron trajectory in the (z, y) plane, where the z position is calculated by $\int_0^\tau v_z dt$. The red, green, and black full diamonds represent $\Omega_i t = 0.1$, 0.6, and 0.77, respectively.

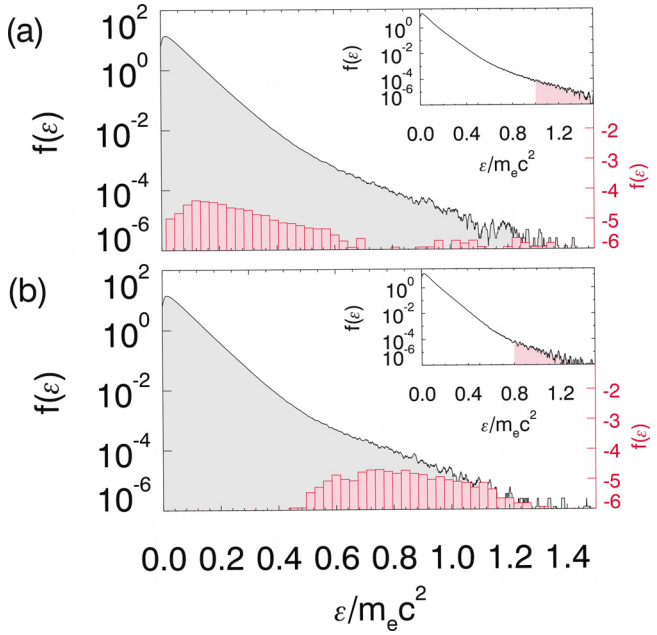

FIG. 9. (a) The energy distributions of electrons at $\Omega_i t = 0.6$, whose energy exceeds $1.0m_ec^2$ at $\Omega_i t = 0.79$ (the flux of non-thermal electrons reaches maximum) in the AP case and is denoted by red color. (b) The energy distribution of electrons at $\Omega_i t = 0.6$, whose energy exceeds $0.8m_ec^2$ at $\Omega_i t = 0.79$ in P case and is denoted by red color. The electron energy spectra at $\Omega_i t = 0.6$ are plotted for reference (black color), and the energy distributions of these electrons at $\Omega_i t = 0.79$ are plotted at the top right corner of each subgraph. The expanding speed is $V_0/c_s = 5$.

During the squeezing stage, the magnetic field in the inflow region is enhanced due to the collision between the two plasma bubbles, and electrons in the magnetic ribbons around the plasma bubbles are heated by the betatron mechanism to form the thermal part of electron energy spectra. At the same time, part of electrons are trapped and bounce between the two approaching plasma bubbles, and they get accelerated mainly by the convective electric field associated with the plasma bubbles, which means that the non-thermal part of electron energy spectra is produced due to the Fermi mechanism. When the expanding speed of plasma bubbles is sufficiently large, the non-thermal electrons form power-law spectra. In the late reconnection stage, electrons can be further accelerated mainly by the reconnection electric field in the diffusion region. Different from the study by Totorica *et al.*,[41] where the reconnection electric field is considered to be the main mechanism to produce energetic electrons, we find that the Fermi mechanism, as well as the reconnection electric field, plays an important role, especially in the squeezing stage.

Magnetic reconnection experiments in a laser-produced plasma have been recently conducted, and energetic electrons are measured in these experiments.[37] These energetic electrons can reach MeVs with a power-law spectrum, and the index is measured to be about 6.5. Here, in this paper, our 2-D PIC simulations show that, when the expanding speed of plasma bubbles is sufficiently large, the formed energy spectra of non-thermal electrons have a power-law distribution, which are accelerated in the squeezing and reconnection stages mainly by the Fermi mechanism and reconnection electric field, respectively. The index of the power-law spectrum is around 5.7 to 6.7 (the expanding speed of the plasma bubbles is $V_0/c_s = 3 - 6$), which is consistent with the experimental observations.[37] Our results also imply that the production of energetic electrons with a power-law distribution cannot be considered as a signature of magnetic reconnection between two expanding plasma bubbles with a high speed because such energetic electrons with a power-law distribution can also be generated from the process of strong squeezing between two plasma bubbles only.

ACKNOWLEDGMENTS

This work was supported by 973 Program (2013CBA01503), the National Science Foundation of China (Grant Nos. 41331067, 41527804, 41121003, and 11220101002), and the Key Research Program of Frontier Sciences, CAS (QYZDJ-SSW-DQC010).

[1]R. G. Giovanelli, Nature **158**, 81 (1946).
[2]S. Tsuneta, Astrophys. J. **456**, 840 (1996).
[3]D. N. Baker, T. I. Pulkkinen, V. Angelopoulos, W. Baumjohann, and R. L. McPherron, J. Geophys. Res. **101**, 12975, doi:10.1029/95JA03753 (1996).
[4]T. Nagai, M. Fujimoto, Y. Saito, S. Machida, T. Terasawa, R. Nakamura, T. Yamamoto, T. Mukai, A. Nishida, and S. Kokubun, J. Geophys. Res. **103**, 4419, doi:10.1029/97JA02190 (1998).
[5]V. Angelopoulos, J. P. McFadden, D. Larson, C. W. Carlson, S. B. Mende, H. Frey, T. Phan, D. G. Sibeck, K. H. Glassmeier, U. Auster, E. Donovan, I. R. Mann, I. J. Rae, C. T. Russell, A. Runov, X. Z. Zhou, and L. Kepko, Science **321**, 931 (2008).
[6]J. A. Wesson, Nucl. Fusion **30**, 2545 (1990).
[7]M. Yamada, F. M. Levinton, N. Pomphrey, R. Budny, J. Manickam, and Y. Nagayama, Phys. Plasmas **1**, 3269 (1994).
[8]R. P. Lin and H. S. Hudson, Sol. Phys. **17**, 412 (1971).
[9]R. P. Lin, S. Krucker, G. J. Hurford, D. M. Smith, H. S. Hudson, G. D. Holman, R. A. Schwartz, B. R. Dennis, G. H. Share, R. J. Murphy, A. G. Emslie, C. Johns-Krull, and N. Vilmer, Astrophys. J. **595**, L69 (2003).
[10]M. Hoshino, T. Mukai, T. Terasawa, and I. Shinohara, J. Geophys. Res. **106**, 25979, doi:10.1029/2001JA900052 (2001).
[11]X. R. Fu, Q. M. Lu, and S. Wang, Phys. Plasmas **13**, 012309 (2006).
[12]P. L. Pritchett, Geophys. Res. Lett. **33**, L13104, doi:10.1029/2005GL025267 (2006).
[13]C. Huang, Q. M. Lu, and S. Wang, Phys. Plasmas **17**, 072306 (2010).
[14]R. S. Wang, Q. M. Lu, C. Huang, and S. Wang, J. Geophys. Res. **115**, A01209, doi:10.1029/2009JA014553 (2010).
[15]M. Y. Wu, C. Huang, Q. M. Lu, M. Volwerk, R. Nakamura, Z. Vörös, T. L. Zhang, and S. Wang, J. Geophys. Res. **120**, 6320, doi:10.1002/2015JA021165 (2015).
[16]H. S. Fu, Y. V. Khotyaintsev, M. André, and A. Vaivads, Geophys. Res. Lett. **38**, L16104, doi:10.1029/2011GL048528 (2011).
[17]M. Y. Wu, Q. M. Lu, M. Volwerk, Z. Vörös, T. L. Zhang, L. C. Shan, and C. Huang, J. Geophys. Res. **118**, 4804, doi:10.1002/jgra.50456 (2013).
[18]C. Huang, M. Y. Wu, Q. M. Lu, R. S. Wang, and S. Wang, J. Geophys. Res. **120**, 1759, doi:10.1002/2014JA020918 (2015).
[19]S. Lu, V. Angelopoulos, and H. S. Fu, J. Geophys. Res. **121**, 9483, doi:10.1002/2016JA022815 (2016).
[20]J. F. Drake, M. Swisdak, H. Che, and M. A. Shay, Nature **443**, 553 (2006).
[21]L. J. Chen, A. Bhattacharjee, P. A. Puhl-Quinn, H. Yang, N. Bessho, S. Imada, S. Mühlbachler, P. W. Daly, B. Lefebvre, Y. Khotyaintsev, A. Vaivads, A. Fazakerley, and E. Georgescu, Nat. Phys. **4**, 19 (2008).
[22]P. L. Pritchett, Phys. Plasmas **15**, 102105 (2008).
[23]M. Oka, T. D. Phan, S. Krucker, M. Fujimoto, and I. Shinohara, Astrophys. J. **714**, 915 (2010).
[24]H. Y. Wang, Q. M. Lu, C. Huang, and S. Wang, Astrophys. J. **821**, 84 (2016).
[25]H. Y. Wang, Q. M. Lu, C. Huang, and S. Wang, Phys. Plasmas **24**, 052113 (2017).
[26]W. Daughton, V. Roytershteyn, H. Karimabadi, L. Yin, B. J. Albright, B. Bergen, and K. J. Bowers, Nat. Phys. **7**, 539 (2011).
[27]H. Q. Song, Y. Chen, G. Li, X. L. Kong, and S. W. Feng, Phys. Rev. X **2**, 021015 (2012).

[28]R. S. Wang, Q. M. Lu, R. Nakamura, C. Huang, A. M. Du, F. Guo, W. L. Teh, M. Y. Wu, S. Lu, and S. Wang, Nat. Phys. **12**, 263 (2016).
[29]Y. Zhao, R. S. Wang, Q. M. Lu, A. M. Du, Z. H. Yao, and M. Y. Wu, J. Geophys. Res. **121**, 10898, doi:10.1002/2016JA023526 (2016).
[30]F. Guo, H. Li, W. Daughton, and Y. H. Liu, Phys. Rev. Lett. **113**, 155005 (2014).
[31]P. M. Nilson, L. Willingale, M. C. Kaluza, C. Kamperidis, S. Minardi, M. S. Wei, P. Fernandes, M. Notley, S. Bandyopadhyay, M. Sherlock, R. J. Kingham, M. Tatarakis, Z. Najmudin, W. Rozmus, R. G. Evans, M. G. Haines, A. E. Dangor, and K. Krushelnick, Phys. Rev. Lett. **97**, 255001 (2006).
[32]P. M. Nilson, L. Willingale, M. C. Kaluza, C. Kamperidis, S. Minardi, M. S. Wei, P. Fernandes, M. Notley, S. Bandyopadhyay, M. Sherlock, R. J. Kingham, M. Tatarakis, Z. Najmudin, W. Rozmus, R. G. Evans, M. G. Haines, A. E. Dangor, and K. Krushelnick, Phys. Plasmas **15**, 092701 (2008).
[33]L. Willingale, P. M. Nilson, M. C. Kaluza, A. E. Dangor, R. G. Evans, P. Fernandes, M. G. Haines, C. Kamperidis, R. J. Kingham, C. P. Ridgers, M. Sherlock, A. G. R. Thomas, M. S. Wei, Z. Najmudin, K. Krushelnick, S. Bandyopadhyay, M. Notley, S. Minardi, M. Tatarakis, and W. Rozmus, Phys. Plasmas **17**, 043104 (2010).
[34]C. K. Li, F. H. Séguin, J. A. Frenje, J. R. Rygg, R. D. Petrasso, R. P. J. Town, P. A. Amendt, S. P. Hatchett, O. L. Landen, A. J. Mackinnon, P. K. Patel, M. Tabak, J. P. Knauer, T. C. Sangster, and V. A. Smalyuk, Phys. Rev. Lett. **99**, 015001 (2007).
[35]M. J. Rosenberg, C. K. Li, W. Fox, I. Igumenshchev, F. H. Séguin, R. P. J. Town, J. A. Frenje, C. Stoeckl, V. Glebov, and R. D. Petrasso, Nat. Commun. **6**, 6190 (2015).
[36]J. Y. Zhong, Y. T. Li, X. G. Wang, J. Q. Wang, Q. L. Dong, C. J. Xiao, S. J. Wang, X. Liu, L. Zhang, L. An, F. L. Wang, J. Q. Zhu, Y. Gu, X. T. He, G. Zhao, and J. Zhang, Nat. Phys. **6**, 984 (2010).
[37]Q. L. Dong, S. J. Wang, Q. M. Lu, C. Huang, D. W. Yuan, X. Liu, X. X. Lin, Y. Li, H. G. Wei, J. Y. Zhong, J. R. Shi, S. E. Jiang, Y. K. Ding, B. B. Jiang, K. Du, X. T. He, M. Y. Yu, C. S. Liu, S. Wang, Y. J. Tang, J. Q. Zhu, G. Zhao, Z. M. Sheng, and J. Zhang, Phys. Rev. Lett. **108**, 215001 (2012).
[38]W. Fox, A. Bhattacharjee, and K. Germaschewski, Phys. Rev. Lett. **106**, 215003 (2011).
[39]S. Lu, Q. M. Lu, Q. L. Dong, C. Huang, S. Wang, J. Q. Zhu, Z. M. Sheng, and J. Zhang, Phys. Plasmas **20**, 112110 (2013).
[40]K. Huang, C. Huang, Q. L. Dong, Q. M. Lu, S. Lu, Z. M. Sheng, S. Wang, and J. Zhang, Phys. Plasmas **24**, 041406 (2017).
[41]S. R. Totorica, T. Abel, and F. Fiuza, Phys. Rev. Lett. **116**, 095003 (2016).
[42]S. Lu, Q. M. Lu, F. Guo, Z. M. Sheng, H. Y. Wang, and S. Wang, New J. Phys. **18**, 013051 (2016).
[43]G. Fiksel, W. Fox, A. Bhattacharjee, D. H. Barnak, P. Y. Chang, K. Germaschewski, S. X. Hu, and P. M. Nilson, Phys. Rev. Lett **113**, 105003 (2014).
[44]S. Lu, Q. M. Lu, C. Huang, Q. L. Dong, J. Q. Zhu, Z. M. Sheng, S. Wang, and J. Zhang, New J. Phys. **16**, 083021 (2014).
[45]Z. Xu, B. Qiao, H. X. Chang, W. P. Yao, S. Z. Wu, X. Q. Yan, C. T. Zhou, X. G. Wang, and X. T. He, Phys. Rev. E **93**, 033206 (2016).